Massachusetts Institute of Technology

Multilayer liquid spreading on superhydrophilic nanostructured surfaces

Rong Xiao, Kuang-Han Chu, and Evelyn N. Wang[a)]

Department of Mechanical Engineering, Massachusetts Institute of Technology, Cambridge, Massachusetts 02139, USA

A phenomenon is presented where a propagating liquid on an array of nanopillars with scalloped features can separate into multiple layers of liquid films. The scallops were found to act as energy barriers that favor liquid separation into several layers over spreading in a uniform film. An analytical model based on surface energy was developed to explain the phenomenon. Additional tailored pillar geometries were fabricated and tested to validate the theory and model. The results provide design guidelines for geometries that promote multiple layer separation and offer opportunities to control liquid film thickness on superhydrophilic surfaces. © *2009 American Institute of Physics*. [DOI: 10.1063/1.3127461]

Nanostructured arrays have received increased interest due to the ability to magnify the intrinsic hydrophobicity or hydrophilicity of a material.[1–6] A significant body of work has focused on the design, analysis, and fabrication of superhydrophobic surfaces, which demonstrated great potential in applications including self-cleaning and drag reduction.[7–13] Recently, there has been growing attention on superhydrophilic surfaces that offer the ability to enhance and manipulate fluid transport in thermal management and biological microfluidic systems.[14–16] The dynamic behavior of liquid spreading on nanostructured surfaces, however, is complex and rich in interfacial phenomena. For example, Courbin *et al.*[17] discovered that the final wetted shape of a spreading droplet (i.e., square, circle, and hexagon) has a strong dependence on the geometric parameters of the topographic features and the intrinsic contact angle. Sbragaglia *et al.*[18] and Pirat *et al.*[19] found that the rate of liquid propagation is typically larger in the direction parallel to the liquid front compared to the direction perpendicular to the liquid front, and depends on the geometry of the surface structures and the intrinsic contact angle. In the previously reported work, the liquid propagated with a layer of uniform thickness across the surfaces. In this letter and in contrast, we report a phenomenon where defined nanostructure geometries cause the liquid to separate into multiple layers with varying thicknesses during the spreading process. Meanwhile, we developed an analytical model to interpret this liquid separation phenomenon and fabricated additional structures to validate the proposed model.

We observed the liquid separation into multiple layers during the propagation across surfaces with silicon nanopillars. An example of such surface structures is shown in the scanning electron micrograph (SEM) in Fig. 1(a). The pillars ranged in diameters from 500 to 800 nm and spacings from 500 to 800 nm and were fabricated by projection lithography and deep reactive ion etching (DRIE). When a 2 μL droplet of de-ionized (DI) water was deposited onto this surface, the liquid separated into several layers. A lower layer advanced first and subsequent sequential layers followed on top of the first one. The phenomenon shown in Fig. 1(b) was visualized

with fluorescent microscopy with a 40× magnification (numerical aperture=0.60). A 29 mM Rhodamine B solution was used to enhance the contrast between the visualized layers. (A movie of the multilayer spreading behavior is provided in supplementary materials S1_Spreading.mpg.[20]) Similar multilayer separation during the receding process was also observed but is not shown here for brevity. The observed horizontal stripes are optical effects due to slight variations in pillar diameter. The multilayer separation appeared to be positively correlated with the presence of the scalloped features on the pillars. When pillar arrays with the same diameter and spacing were fabricated but with nonvisible scalloped features, the liquid spread across the surface with a uniform thickness. These observations motivated us to develop a surface-energy-based model to predict liquid separation induced by the fine structures on the nanopillars.

In the model, the scallops are idealized into tiered steps, as shown in Fig. 2(a). The parameters h_u, h_l, d_u, and d_l are the upper and lower height, and the upper and lower diameter, respectively. Figure 2(b) shows the normalized change in surface energy as a function of the normalized liquid height. Because the pillars are hydrophilic, a higher liquid height typically corresponds to a lower surface energy as shown between state (i) and state (ii), as well as between state (iii) and state (iv). However, when a horizontal surface is present, an energy barrier exists as shown between state (ii) and state (iii). In this case, when the liquid covers the surface, the amount of surface energy gained from the solid-
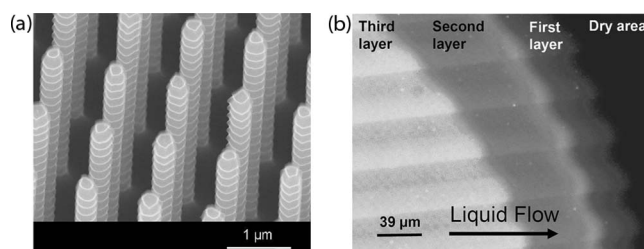

FIG. 1. (a) SEM of a surface with nanostructured arrays of pillars with diameters of 500 nm and spacings of 800 nm. The scallops have dimensions of approximately 100 nm. (b) Visualization of multilayer spreading on the corresponding geometry in (a). Liquid spreads from left to right where the dark area is dry. The differences in intensity indicate variations in liquid film thickness.

[a)]Author to whom correspondence should be addressed. Electronic mail: enwang@mit.edu.
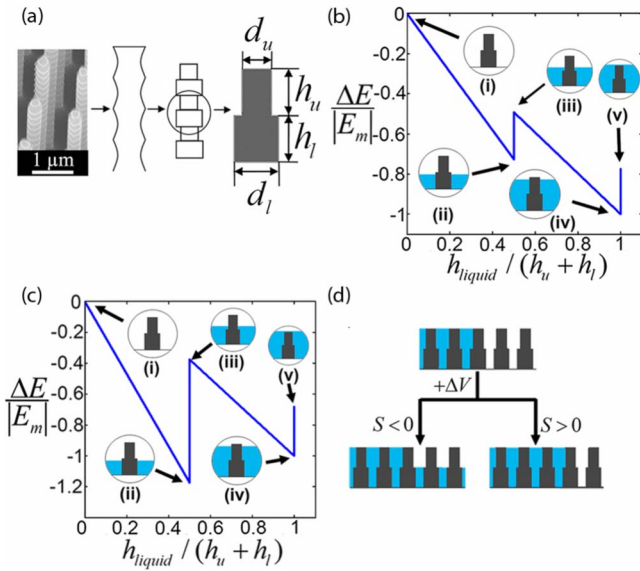
94, 193104-1

FIG. 2. (Color online) (a) Schematic showing the idealization of the scalloped pillars from the DRIE process into tiered steps. (b) The change in normalized surface energy as a function of normalized liquid height on a two-tiered pillar geometry where $h_u = h_l$ and $d_u = 0.7 d_l$. E_m is the energy change when the liquid wets the entire pillar and h_{liquid} is the height of the liquid interface. (c) The change in normalized surface energy as a function of normalized liquid height on a two-tiered pillar geometry where $h_u = h_l$ and $d_u = 0.5 d_l$. (d) Schematic showing a liquid droplet deposited onto the surface and the two possible spreading configurations determined by the parameter S when a volume of ΔV is supplied from the droplet.

liquid and liquid-air interfaces is greater than the surface energy lost due to the reduced solid-air interface. A similar energy barrier is present between state (iv) and state (v), which maintains the liquid below the top of the pillars. Figure 2(b) shows a particular configuration with naturally oxidized silicon pillars with an intrinsic contact angle of 38° and with $h_u = h_l$ and $d_u = 0.7 d_l$. The size of the energy barrier between state (ii) and state (iii) scales with the intrinsic contact angle and $1 - (d_u/d_l)^2$. Therefore, for pillars of the same material (same intrinsic contact angle), a decrease in the d_u/d_l ratio will increase the size of this energy barrier such that state (iv) can have a higher energy than state (ii). One example of such a case is shown in Fig. 2(c), when $h_u = h_l$ and $d_u = 0.5 d_l$. The difference in the normalized energy between state (ii) and state (iv) plays an important role in the separation phenomena, which is determined by

$$S = \gamma_{LV} \frac{1}{h_u + h_l} \left(\frac{1}{\Lambda_1} - \frac{1}{C} \right) - \gamma_{LV} \frac{1}{h_u + h_l} \cos\theta \left(\frac{1}{\Lambda_1} - \frac{1}{C} \right)$$
$$- \gamma_{LV} \frac{1}{l} \cos\theta \left\{ \frac{\pi A [C + B(1 - C)]}{\Lambda_2} - \frac{\pi A}{1 - \pi A^2/4} \right\},$$

$$\Lambda_1 = (1 - C) + \frac{(1 - \pi A^2/4)}{(1 - \pi A^2 B^2/4)} C, \tag{1}$$

$$\Lambda_2 = \left(1 - \frac{\pi A^2 B^2}{4} \right)(1 - C) + \left(1 - \frac{\pi A^2}{4} \right) C,$$

where $A = d_l/l$, $B = d_u/d_l$, $C = h_l/(h_u + h_l)$, l is the distance between the centers of neighboring pillars, γ_{LV} is the surface tension of the liquid, and θ is the intrinsic contact angle of the liquid on the solid. The details of the derivation are provided in supplementary materials S_2.[20] When the liquid is deposited onto the surface, as shown in Fig. 2(d), the liquid chooses the configuration with the lower surface energy. If $S < 0$, the energy of state (ii) is lower than that of state (iv) and when a small volume of liquid ΔV is supplied from the droplet in this case, the liquid propagates at the edge as a separated layer [Fig. 2(d) left configuration]. In contrast, when $S > 0$, state (iv) is preferred because it has the lowest energy and the liquid remains in a uniform layer at the height of the pillars [Fig. 2(d) right configuration].

The analytical curve for $S = 0$, as calculated from Eq. (1), is plotted in Figs. 3(b) and 3(c). For the case considered, $\gamma_{LV} = 0.072$ N/m and $\theta = 38°$ (where the contact angle was measured for a smooth naturally oxidized silicon surface with a goniometer). The cases for Figs. 3(b) and 3(c) differ in the location of the lower edge, resulting in $C = 0.63$ and $C = 0.49$, respectively. These two cases were chosen to facilitate a comparison with the experiment described below. The $S = 0$ curve demarcates the boundary between single-layer and dual-layer spreading in the parameter space of A and B.

To validate the model, additional pillars with a single notch of defined size d_u and location h_l were fabricated [Fig. 3(a)]. The etching recipe is provided in supplementary materials S_3.[20] The total height of the pillars is 5 μm. The lower diameter d_l ranges from 2 to 3.5 μm while the distance between pillars l ranges from 2 to 7 μm, yielding a variation in parameter A from 0.2 to 0.7. However, d_u, and hence the parameter B, is limited to a range of 0.7 to 0.9 from the availability of existing DRIE capabilities. We fabricated the
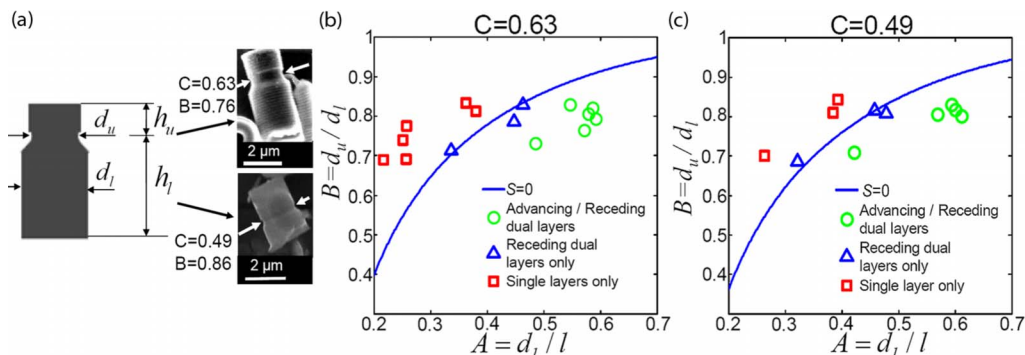

FIG. 3. (Color online) (a) Schematic showing pillars with a single notch and associated dimensions. Representative SEMs are shown for the cases when $C = 0.63$, $B = 0.76$, $C = 0.49$, and $B = 0.86$. (b) The parameter space that determines the presence of a single or dual layers for the case $C = 0.63$. Experiments with pillars of diameters ranging from 2 to 3.5 μm and spacings of 2 to 7 μm are plotted. (c) Parameter space that determines the presence of single or dual layers for the case $C = 0.49$. The range of diameters and the spacings are the same as in (b).

notch at two heights, 3.15 and 2.45 μm, which resulted in $C=0.63$ and $C=0.49$, respectively. SEM images of representative pillars with a single notch are shown in Fig. 3(a). The working liquid used was DI water. The experimental results are overlayed with the model predictions in Figs. 3(b) and 3(c). The cases where dual layers appeared in both advancing and receding processes are specified as circles. Interestingly, we observed that for certain pillar geometries, dual-layer separation occurred only during the receding process and not during the advancing process. These cases are labeled as triangles. Pillar geometries in which the liquid advanced and receded in a uniform layer are labeled as squares.

The experimental results show that the theoretical curve well demarcates the boundaries between geometries that lead to separated layers, and those that lead to a single layer, for both the advancing and receding processes. However, close to the boundary ($S=0$), liquid separation occurs only in the receding process (the triangles). This result is expected as briefly explained below. The analytical model we developed only accounted for surface energy. However, in our experiment, when the droplet was deposited, the Laplace pressure from the positive curvature of the droplet also contributed to the advancing process of the liquid. As a result, the liquid has a higher kinetic energy which enables the liquid to overcome the energy barrier for S close to zero. In the receding process, the liquid evaporated and receded slowly; the liquid is thus only driven by surface tension and leads to liquid separation. Liquid separation is, therefore, well predicted by the theory. The spreading behavior for geometries far from the boundary is not affected by the additional effect of the Laplace pressure and the model is considered accurate in predicting both advancing and receding behaviors.

In summary, nanoscale pillars with scallops of particular geometries can induce energy barriers that lead to a disruption of the liquid upon spreading, forming multilayer liquid films. A model based on surface energy was developed to explain the observations. Despite the idealizations that were made on the geometry, the theoretical prediction provides good agreement with the experimental observations. The results suggest that the spreading behavior can be controlled by choosing proper pillar geometries, which offer possibilities to control the thickness of liquid films on textured surfaces.

[1] R. N. Wenzel, Ind. Eng. Chem. **28**, 988 (1936).
[2] A. B. D. Cassie and S. Baxter, Trans. Faraday Soc. **40**, 546 (1944).
[3] R. D. Hazlett, J. Colloid Interface Sci. **137**, 527 (1990).
[4] N. A. Patankar, Langmuir **20**, 7097 (2004).
[5] E. Martines, K. Seunarine, H. Morgan, N. Gadegaard, C. D. W. Wilkinson, and M. O. Riehle, Nano Lett. **5**, 2097 (2005).
[6] C. W. Extrand, Langmuir **21**, 10370 (2005).
[7] Z. Yoshimitsu, A. Nakajima, T. Watanabe, and K. Hashimoto, Langmuir **18**, 5818 (2002).
[8] N. A. Patankar, Langmuir **20**, 8209 (2004).
[9] J. Jopp, H. Grull, and R. Yerushalmi-Rozen, Langmuir **20**, 10015 (2004).
[10] R. Furstner, W. Barthlott, C. Neinhuis, and P. Walzel, Langmuir **21**, 956 (2005).
[11] W. Li and A. Amirfazli, Adv. Colloid Interface Sci. **132**, 51 (2007).
[12] A. Tuteja, W. Choi, M. L. Ma, J. M. Mabry, S. A. Mazzella, G. C. Rutledge, G. H. McKinley, and R. E. Cohen, Science **318**, 1618 (2007).
[13] A. Ahuja, J. A. Taylor, V. Lifton, A. A. Sidorenko, T. R. Salamon, E. J. Lobaton, P. Kolodner, and T. N. Krupenkin, Langmuir **24**, 9 (2008).
[14] A. P. Blanchard, R. J. Kaiser, and L. E. Hood, Biosens. Bioelectron. **11**, 687 (1996).
[15] F. C. Cebeci, Z. Z. Wu, L. Zhai, R. E. Cohen, and M. F. Rubner, Langmuir **22**, 2856 (2006).
[16] C. W. Extrand, S. I. Moon, P. Hall, and D. Schmidt, Langmuir **23**, 8882 (2007).
[17] L. Courbin, E. Denieul, E. Dressaire, M. Roper, A. Ajdari, and H. A. Stone, Nature Mater. **6**, 661 (2007).
[18] M. Sbragaglia, A. M. Peters, C. Pirat, B. M. Borkent, R. G. H. Lammertink, M. Wessling, and D. Lohse, Phys. Rev. Lett. **99**, 156001 (2007).
[19] C. Pirat, M. Sbragaglia, A. M. Peters, B. M. Borkent, R. G. H. Lammertink, M. Wessling, and D. Lohse, Europhys. Lett. **81**, 66002 (2008).
[20] See EPAPS Document No. E-APPLAB-94-024918 for the movie of the multilayer spreading behavior, the derivation of the equation, and the etching recipes. For more information on EPAPS, see http://www.aip.org/pubservs/epaps.html.